RSC Advances

PAPER

View Article Online
View Journal | View Issue

Cite this: *RSC Adv.*, 2020, **10**, 44876

Effect of $CaCO_3$ on catalytic activity of Fe–Ce/Ti catalysts for NH_3-SCR reaction

Xiaobo Wang, *[ab] Qiuyue Fang,[a] Jia Wang,*[c] Keting Gui[d] and Hywel Rhys Thomas[b]

Received 27th August 2020
Accepted 30th November 2020

DOI: 10.1039/d0ra07351b

rsc.li/rsc-advances

In the present work, fresh and Ca poisoned Fe–Ce/Ti catalysts were prepared and used for the NH_3-SCR reaction to investigate the effect of Ca doping on the catalytic activity of catalysts. And these catalysts were characterized by BET, XRD, Raman, UV-vis DRS, XPS, H_2-TPR, and NH_3-TPD techniques. The obtained results demonstrate that Ca doping could lead to an obvious decrease in the catalytic activity of catalysts. The reasons for this may be due to the smaller specific surface area and pore volume, the decreased ratio of Fe^{3+}/Fe^{2+} and Ce^{3+}/Ce^{4+}, as well as the reduced redox ability and surface acidity.

Introduction

The emission of NO_x from stationary sources including coal-fired power plants and industrial boilers has caused several environmental problems such as photo-chemical smog and acid rain.[1,2] It has been proved that the effective technology for purifying NO emission is the selective catalytic reduction of NO_x with NH_3.[3] At present, the widely used commercial catalysts for this process are V_2O_5/TiO_2 and V_2O_5–WO_3/TiO_2, which can yield superior catalytic activity in the range of 300–400 °C.[4] However, these catalysts also possess some disadvantages such as the toxicity of VO_x to the ecosystem and the conversion of SO_2 to SO_3 at high temperature.[5,6] Therefore, it is of great demand to develop the catalysts without the drawbacks mentioned above.

For this purpose, many catalysts containing metal oxides have been found to possess high catalytic activity for SCR reaction including Fe, Ce, Mn, and Cu based catalysts.[7–21] Based on our previous study, we found the Fe–Ce/Ti catalysts could exhibit high catalytic activity for the NH_3-SCR reaction. However, there are several components in the real flue gases including K, Ca, CO_2, and SO_2, which will lead to the physical or chemical deactivation of catalysts and thus restrict the industrial application of catalysts. For the Ca poisoning on the SCR catalysts, it is reported that the catalytic activity of catalysts will display an obvious decrease when the amount of CaO reached to 2 wt% on the catalyst surface.[22,23] To reveal Ca poisoning on the catalysts, much research has focused on this topic and achieved different views on it. For example, Zhu *et al.* found the introduction of Ca could lead to a great loss of catalytic activity over the Cu-SSZ-39 catalyst due to the decrease of acid sites and conversion of isolated Cu^{2+} ions to $CuAlO_x$ and CuO_x species.[24] Odenbrand attributed the deactivation of the V_2O_5–WO_3/TiO_2 catalyst caused by the $CaSO_4$ to a chemical phenomenon, not the changes of the BET surface area or the pore structure of the catalyst.[25] Chang *et al.* reported that the overoxidation of NH_3 was regarded as one significant reason for the decrease of catalytic activity over the $CaBr_2$ poisoned commercial V_2O_5–WO_3/TiO_2 catalyst.[26] While Liu *et al.* revealed that, besides the inhibition of NH_3 adsorption, the deactivation of $Ca(NO_3)_2$ poisoned Ce/TiO_2 catalyst was due to the NO oxidation and suppressed NH_3 activation.[27] Based on the results above, it can be seen that the addition of Ca undoubtedly leads to the deactivation of catalysts. Nevertheless, the reason and behavior for the deactivation over different catalysts are different. Especially for the Fe–Ce/TiO_2 catalyst, the deactivation behavior of catalysts resulted from the addition of $CaCO_3$ is still undetermined and whether such deactivation is attributed to the physical or chemical phenomenon or both is still unclear. Furthermore, the relationship between the activity loss and the changes of textures, redox/acid properties, and surface characteristics of the $CaCO_3$ poisoned catalysts remains lacking of report.

Therefore, in this work, the fresh Fe–Ce/Ti catalyst and the catalyst with different loading of $CaCO_3$ were prepared and used for SCR of NO with NH_3. The effect of $CaCO_3$ on the catalytic activity of Fe–Ce/Ti catalyst was investigated and the deactivation effect caused by $CaCO_3$ was explored by many characterization methods including BET, XRD, Raman, UV-vis DRS, XPS, H_2-TPR and NH_3-TPD techniques from the aspects of physicochemical properties of the catalyst.

[a]*School of Environmental Science, Nanjing Xiaozhuang University, Nanjing 211171, Jiangsu, China. E-mail: xb_wang88@126.com*

[b]*Geoenvironmental Research Centre, School of Engineering, Cardiff University, Cardiff, CF24 3AA, UK*

[c]*College of Chemical Engineering, Nanjing Forestry University, Nanjing 210037, Jiangsu, China. E-mail: wangjia_njfu@163.com*

[d]*School of Energy and Environment, Southeast University, Nanjing 210096, Jiangsu, China*

Experimental

Catalyst preparation

Preparation of Fe–Ce/Ti catalyst. To the fully stirred (450 rpm on a magnetic heating stirrer) suspension (solution) of 18.04 g $Fe(NO_3)_3 \cdot 9H_2O$, 58.17 g $Ce(NO_3)_3 \cdot 6H_2O$, and 200 mL deionized water, 25 g TiO_2 was added. To the resulting mixture, an ammonia

solution was added at 50 °C until the pH reached 10 and stirred for 2 h at 50 °C. The resulting solution was dried at 120 °C and then the sample was powdered and calcined at 450 °C for 5 h.

Preparation of $CaCO_3$ poisoned catalysts. To the stirred (450 rpm on a magnetic heating stirrer) suspension of 15 g Fe–Ce/Ti catalyst in 80 mL deionized water, the calculated amount of $Ca(OH)_2$ and $(NH_4)_2CO_3$ was added and the resulted mixture was stirred for 1 h at 50 °C. And then the sample was dried at 120 °C and calcined at 450 °C for 3 h. At last, the catalyst could be gained after ground, tableted, and sieved to 30–60 mesh for activity measurement. The catalysts with different loading of $CaCO_3$ were designated as Ca-1, Ca-2, and Ca-3, respectively, where the number 1, 2, and 3 represented the mass percentage of Ca based on the fresh catalyst.

Catalyst characterization

The specific surface area, pore volume and pore diameter of catalysts were obtained by N_2 adsorption–desorption isotherms on an ASAP 2460 instrument at −196 °C (Micrometrics, USA).

The crystal structure of catalysts was observed on a SmartLab 9 X-ray diffractometer (Cu Kα radiation, $\lambda = 0.15418$ nm) in the angle of 10–90°.

The Raman measurements were carried out on a Thermo Scientific DXR 2xi Raman spectrometer using an excitation source of laser radiation at 532 nm.

The UV-vis diffuse reflectance spectroscopy (DRS) was performed on a Shimadzu UV-3600 PC spectrophotometer with an integrating sphere at room temperature and the spectra were recorded from 200–800 nm.

The surface oxidation states of catalysts were explored by the X-ray photoelectron spectroscopy (XPS) on Thermo Fisher Scientific EXCALAB 250Xi instrument and the binding energy was calculated by a C 1s peak (284.8 eV).

The redox properties and surface acidity of catalysts were gained by H_2-temperature programmed reduction experiments and NH_3-temperature programmed desorption (NH_3-TPD) experiments on an AutoChem II 2920 (Micromeritics, USA) chemical adsorption instrument, respectively. For each H_2-TPR experiment, about 50 mg sample was used and pretreated in N_2 at 300 °C for 2 h. After cooled to room temperature and stabilization, the H_2-TPR data was recorded from 50–500 °C with a heating rate of 10 °C min^{-1}. For the NH_3-TPD experiments, after pretreatment of 50 mg sample in N_2 at 300 °C for 2 h, the sample was cooled to 50 °C and treated with 10% NH_3/He for 1 h, and followed by the He-purge for 1 h. At last, the data was collected from 50 to 500 °C at 10 °C min^{-1} under the He atmosphere.

Catalyst activity evaluation

The SCR catalytic activity of catalysts was evaluated using a fixed bed reactor with 5 mL catalyst in the temperature range of 120–360 °C. The simulated steam with a total flow rate of 1.5 L min^{-1} consisted of 500 ppm NO, 500 ppm NH_3, 3% O_2, and N_2 as the balance. The concentrations of the outlet gases were monitored by a flue gas analyzer (RBR ECOM-J2KN) online.

NO conversion was calculated according to the following equation:

$$C_{NO} = \frac{[NO]_{inlet} - [NO]_{outlet}}{[NO]_{inlet}} \times 100 \quad (1)$$

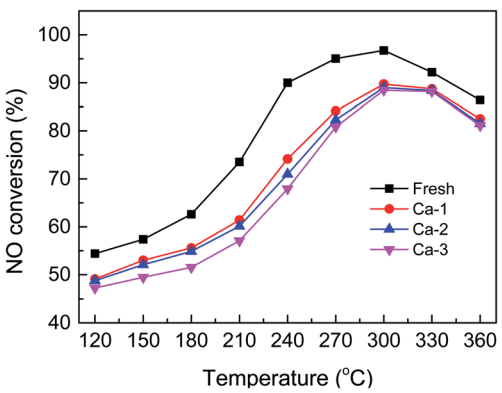

Fig. 1 NO conversion over the fresh and different Ca-poisoned catalysts.

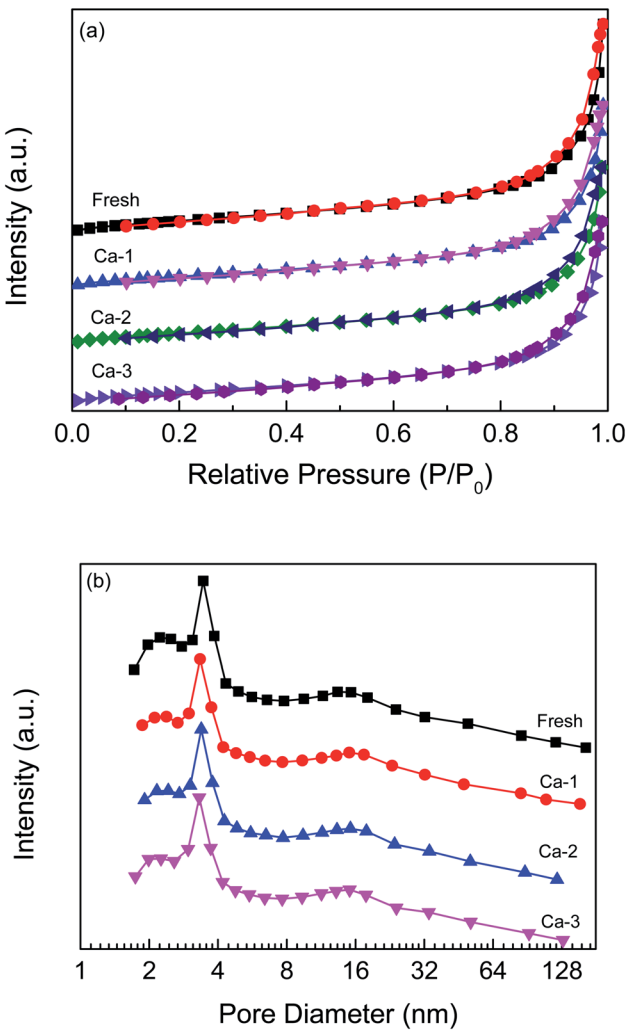

Fig. 2 N_2 adsorption–desorption isotherms (a) and pore size distributions (b) of the fresh and different Ca-poisoned catalysts.

Table 1 The textual properties of the fresh and different Ca-poisoned catalysts

Catalysts	S_{BET} (m^2 g^{-1})	Pore volume (mm^3 g^{-1})	Pore diameter (nm)
Fresh	35.79	0.14	14.88
Ca-1	30.35	0.12	15.05
Ca-2	31.33	0.12	14.51
Ca-3	29.48	0.12	14.80

Table 2 The crystal properties of the fresh and different Ca-poisoned catalysts

	2θ (°)	
Catalysts	TiO_2 (1 0 1) plane	CeO_2 (1 1 1) plane
Fresh	25.35	28.79
Ca-1	25.35	28.81
Ca-2	25.34	28.82
Ca-3	25.35	28.85

Results and discussions

Catalytic activity of catalysts

The catalytic activity of the fresh and Ca-poisoned Fe–Ce/Ti catalysts are displayed in Fig. 1. It can be seen that the fresh catalyst exhibits the best catalytic activity in the whole temperature range and more than 90% NO conversion could be obtained from 240 to 330 °C. When Ca was introduced into the Fe–Ce/Ti catalyst, the catalytic activity shows a significant decrease, indicating the deactivation occurs after Ca doping. For the Ca-1 catalyst, the highest catalytic activity is no more than 90% in the whole temperature range tested. And loading with 2% and 3% Ca lead to a more serious decrease in catalytic activity and the Ca-3 catalyst yields the lowest NO conversion, which demonstrates that the deactivation of the catalysts becomes more and more serious as the loading of Ca increases.

Results of BET analysis

The N_2 adsorption–desorption isotherms and pore size distributions of the fresh and Ca-poisoned catalysts are displayed in Fig. 2. All the isotherms present a typical IV curve with a hysteresis loop of H3-type, suggesting the presence of the mesopore structure of catalysts.[28–30] As shown in Fig. 2(b), the pore diameters of the fresh and Ca-poisoned catalysts are all in the mesopores range of 2–30 nm and the pore diameters of catalysts are not greatly changed after the doping of different amounts of Ca. The specific surface area, pore volume and pore diameter of the fresh and different Ca-poisoned catalysts are listed in Table 1. For the fresh catalyst, the specific surface area and pore volume are 35.79 m^2 g^{-1} and 0.14 mm^3 g^{-1}, respectively. After the doping of Ca, the specific surface area and pore volume of the Ca-poisoned catalysts both are decreased. A catalyst with a smaller specific surface area and pore volume would not provide enough and suitable active sites on the catalyst surface, which is not conducive to promote the adsorption of reactant molecules and thus can reduce the catalytic activity of the catalyst.

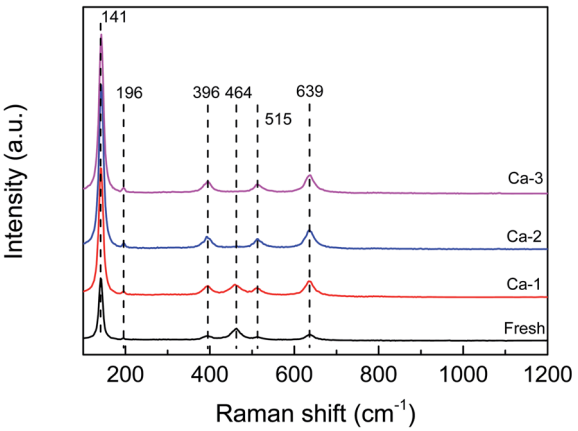

Fig. 4 Raman spectra of the fresh and different Ca poisoned catalysts.

Results of XRD analysis

The phases structure of catalysts was detected and the results are depicted in Fig. 3. It can be seen that several strong diffraction peaks attributed to TiO_2 (anatase) and CeO_2 can be

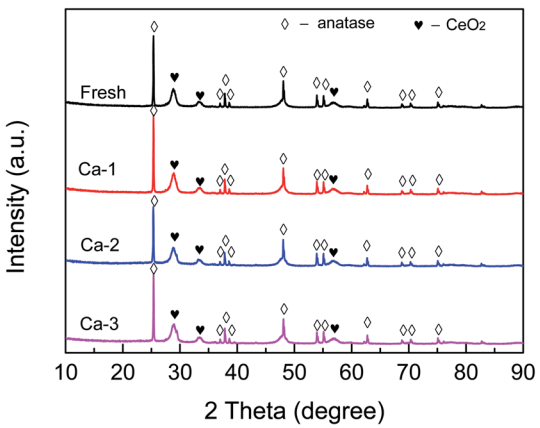

Fig. 3 XRD patterns of the fresh and different Ca-poisoned catalysts.

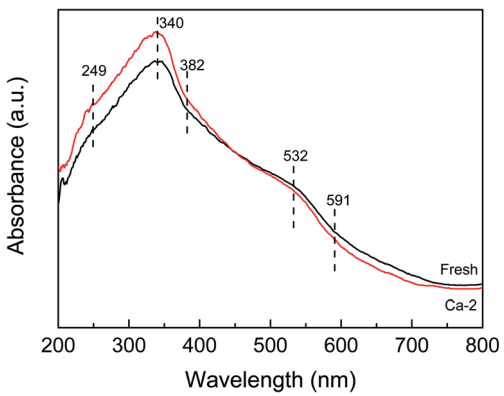

Fig. 5 UV-vis DRS spectra of the fresh and the Ca-2 catalysts.

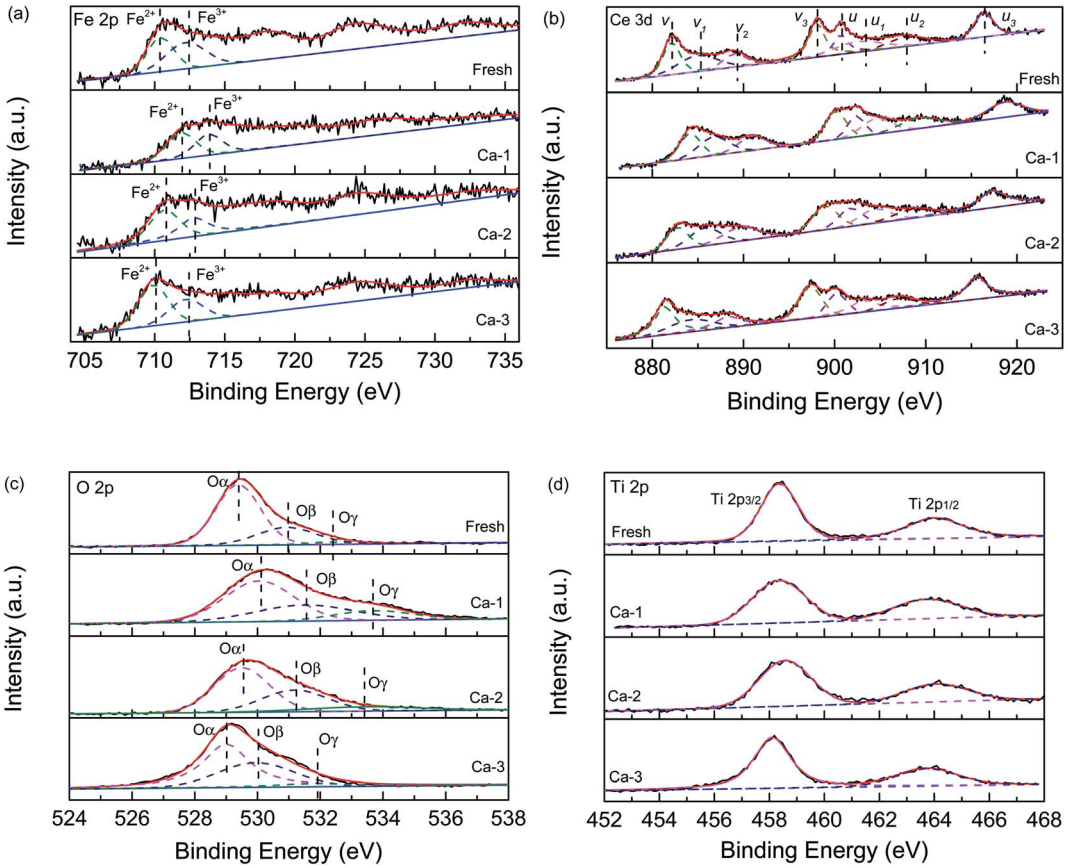

Fig. 6 XPS spectra of the fresh and different Ca poisoned catalysts: (a) Fe 2p, (b) Ce 3d, (c) O 1s and (d) Ti 2p.

observed for all the catalysts. Meanwhile, no characteristic peaks of Fe species can be detected for the studied catalysts, indicating that the iron species are in an amorphous structure or dispersed well. Moreover, as listed in Table 2, the positions of (1 0 1) plane of anatase TiO_2 over the fresh and Ca-poisoned catalysts are basically not changed after the doping of Ca, which indicates that the doped Ca could not interact with Ti and thus affect the crystallographic parameter of TiO_2. However, compared with that of the fresh catalyst, the position of (1 1 1) plane of CeO_2 over different Ca-poisoned catalysts all are shifted. The results demonstrate that the doped Ca leads to the expansion of the CeO_2 crystal unit, which may be due to the Ca^{2+} is partly doped into the original lattice.

Results of Raman analysis

The Raman analysis was performed to detect the structural changes due to the doping of Ca and the results are displayed in Fig. 4. For the fresh catalyst, the Raman peaks at 141, 196, 396, 515 and 639 cm^{-1} could be observed and are ascribed to the anatase TiO_2.[31–33] Besides these, an obvious peak at 464 cm^{-1} can be detected over the fresh catalyst, which may be assigned to the F_{2g} vibration modes of CeO_2.[34,35] Furthermore, no characteristic Raman peaks of Fe oxide species are observed over the fresh catalyst, indicating the Fe oxide species exist as amorphous structure or are dispersed well on the TiO_2 support's surface. These results are consistent well with the XRD results. For the Ca doping catalysts, the same Raman signals attributed to the anatase TiO_2 as the fresh catalyst can be observed and the intensity becomes stronger with the increase of the Ca loading, suggesting that the Ca doping could promote the crystallization of TiO_2. And by contrast, the peak assigned to the CeO_2 at

Table 3 Surface atomic concentrations (%) and the atomic ratios of Fe^{3+}/Fe^{2+} and Ce^{3+}/Ce^{4+} over the different catalysts

Catalysts	Fe	Ce	Ti	Ca	O	Fe^{3+}/Fe^{2+}	Ce^{3+}/Ce^{4+}
Fresh	4.83	3.56	7.70	—	37.11	1.13	0.38
Ca-1	3.72	3.07	6.49	1.67	35.01	0.81	0.35
Ca-2	3.71	2.45	6.25	2.07	32.35	0.77	0.33
Ca-3	2.52	2.78	5.67	2.57	33.78	0.63	0.29

Table 4 The XPS fitting data of O 1s of the fresh and different Ca-poisoned catalysts

	Atomic ratio (%)		
Catalysts	O_α/O	O_β/O	O_γ/O
Fresh	68.99	26.81	4.20
Ca-1	55.18	30.30	14.52
Ca-2	55.97	32.73	11.30
Ca-3	57.51	35.37	7.10

464 cm^{-1} becomes weaker and broader and even disappears with the increase of Ca loading, which may be due to the coverage of the CeO_2 surface by the Ca species. Concerning the Fe oxide species, no peaks belonged to the Fe oxide species could be detected over the Ca doped catalysts either.

Results of UV-vis DRS analysis

The UV-vis spectra of the fresh and Ca-2 catalysts are displayed in Fig. 5. Both of the spectra exhibit similar shapes with the same adsorption bands. The absorption band at 340 nm and that below 300nm may be attributed to the $Ce^{4+} \leftarrow O^{2-}$ and $Ce^{3+} \leftarrow O^{2-}$ charge transfer (249 nm) overlapped with the isolated Fe^{3+}, respectively.[36–39] While the absorption band at 382 nm and above 400 nm (532 and 591 nm) is ascribed to the oligomeric clusters, and large Fe_2O_3 particles, respectively.[39,40] Despite they possess the same absorption bands, the absorption edge of the fresh and the Ca-2 catalyst is determined to be different. It is 473 nm for the fresh catalysts, while it is calculated to be 464 nm for the Ca-2 catalyst, indicating the doping of Ca will lead to an obvious blue-shift owing to the changes in the metallic species environment.[41] The decreased adsorption edge may increase the energy band gap, which will not be beneficial for accelerating the oxygen transfer rate and promoting the catalytic activity of catalyst.[42] Therefore, the doping of Ca leads to a higher energy band gap, which corresponds to reduced redox properties for the Ca poisoned catalysts.

Results of XPS analysis

The XPS measurement was used to detect the effect of Ca doping on the chemical states of elements over the different catalysts. Fig. 6(a) displays the Fe 2p spectra of the fresh and different Ca poisoned catalyst. It can be seen that all of the spectra contained two peaks, which can be ascribed to the Fe^{3+} and Fe^{2+}, respectively.[6,21,43] As listed in Table 3, the ratio of Fe^{3+}/Fe^{2+} over the fresh catalyst is calculated to be 1.13 from the peaking fitting result, while it is 0.81, 0.77, and 0.63 for the Ca-1, Ca-2, and Ca-3 catalyst, respectively. The redox reaction of $Fe^{2+} + Ce^{4+} \leftrightarrow Fe^{3+} + Ce^{3+}$ can generate Fe^{3+} and Ce^{3+} and create charge imbalance over the catalyst's surface. The higher contents of Fe^{3+} can facilitate the oxidation of NO to NO_2, which will stimulate the "fast SCR" reaction and thus promote the catalytic activity of catalysts.[44,45] The XPS results show that the Fe^{3+} contents are greatly decreased due to the doping of Ca and the more the Ca doped, the more serious the downward trend is. The reduced Fe^{3+} will lower the catalytic reduction of NO and thus lead to the poor catalytic performance of catalysts.

Table 5 H_2-TPR quantitative data of different catalysts

Catalysts	The temperature of reduction peaks (°C) T_1	T_2	T_3	T_4	Total H_2 consumption (a.u.)
Fresh	266	328	380	469	0.89
Ca-1	329	374	409	466	0.76
Ca-2	336	380	416	474	0.76
Ca-3	332	375	410	465	0.59

The Ce 3d spectra of different catalysts are exhibited in Fig. 6(b) and all can be divided into eight sub-peaks. The sub-peaks denoted as u_1 and v_1 are assigned to the Ce^{3+}, while other peaks u, u_1, u_2, v, v_1, and v_2 are related to the Ce^{4+}.[46] This result indicates that the Ce^{3+} and the Ce^{4+} are coexistence over the catalyst surface. However, as listed in Table 4, the ratio of Ce^{3+}/Ce^{4+} of the four studied catalysts is different. For the fresh catalyst, it possesses the highest ratio of Ce^{3+}/Ce^{4+} and the sequence of the ratio of Ce^{3+}/Ce^{4+} is ranked by fresh (0.38) > Ca-1 (0.35) >Ca-2 (0.33) > Ca-3 (0.29) catalyst, which is well consistent with the catalytic activity of the catalysts. It is well known that more Ce^{3+} will promote the formation of oxygen vacancies and unsaturated chemical bonds *via* creating a charge imbalance and thus accelerate the catalytic activity of catalyst.[47,48] Therefore, the decreased Ce^{3+} resulted from the Ca doping may be one reason for the reduced catalytic activity of the catalyst. Besides these, the Ce^{3+} can exert great effect on the surface acidity of catalyst and more Ce^{3+}content will promote

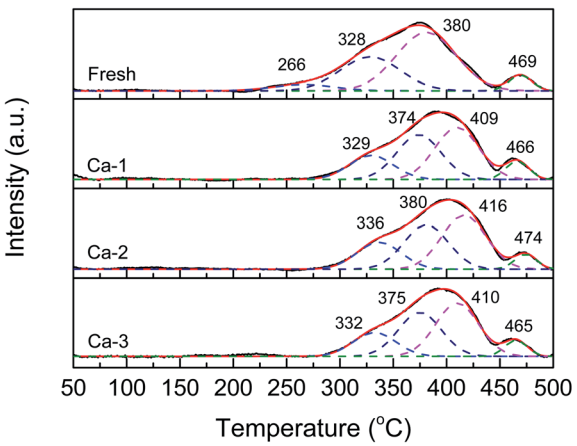

Fig. 7 H_2-TPR profiles of the fresh and different Ca-poisoned catalysts.

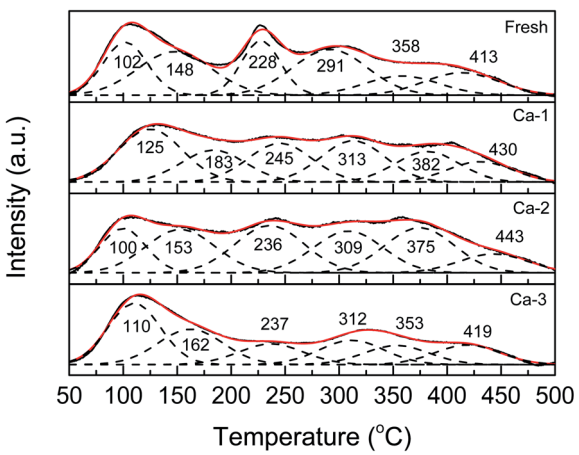

Fig. 8 NH_3-TPD profiles of the fresh and different Ca poisoned catalysts.

Table 6 NH_3-TPD quantitative data of different catalysts

	The temperature of desorption peaks (°C)						Surface acidity (mmol g^{-1})		
Catalysts	Peak 1	Peak 2	Peak 3	Peak 4	Peak 5	Peak 6	Weak	Medium	Total
Fresh	102	148	228	291	358	413	0.54	0.15	0.69
Ca-1	125	183	245	313	382	430	0.23	0.18	0.41
Ca-2	100	153	236	309	375	443	0.27	0.24	0.51
Ca-3	110	162	237	312	353	419	0.30	0.17	0.47

the adsorption of ammonia and thus enhance the catalytic activity of catalyst.[48,49] This conclusion is supported by the NH_3-TPD results discussed below. And this may be another reason for the decrease of catalytic performance for the Ca poisoned catalysts.

Fig. 6(c) shows the O 1s curves of the fresh and different Ca poisoned catalysts. All spectra could be separated into three peaks, which are attributed to the lattice oxygen (O_α), the surface chemisorbed oxygen (O_β), and the adsorbed water (O_γ), respectively. And as listed in Table 4, the O_β over the fresh catalyst is 26.81%, while this value respectively is 30.30, 32.73, and 35.37% for the Ca-1, Ca-2, and Ca-3 catalyst. These results suggest that the doping of Ca will lead to an increase of the surface chemisorbed oxygen over the catalyst's surface. It was reported that the more surface chemisorbed oxygen will facilitate the catalytic activity of catalysts than that of the lattice oxygen.[50] However, it is not the case for the Ca doped catalysts. The more surface chemisorbed oxygen maybe leads to side reaction during the SCR reaction, which will result in a decrease in the catalytic performance of the catalyst. Besides this, the catalytic activity of the catalyst is affected by many other factors including textural properties, surface acidity, and redox ability.

Results of H_2-TPR analysis

The H_2-TPR profiles of the fresh and different Ca poisoned catalysts are displayed in Fig. 7. And the temperature of reduction peaks and the total H_2 consumption calculated by the peak area are listed in Table 5. It can be seen from Fig. 7 that all the H_2-TPR curves display the same shapes and can be divided into four reduction peaks in the temperature range of 100–500 °C, which represents the reduction of different reducible species. For the fresh catalyst, the peaks centered at 266 and 328 °C may be assigned to the reduction of surface and sub-surface Fe_2O_3 to Fe_3O_4, and the peaks at 380 and 469 °C may be ascribed to the reduction of surface CeO_2 and Fe_3O_4 to FeO, respectively.[51–55] After the doping of Ca, the H_2-TPR profiles of the Ca poisoned catalysts are similar to the fresh catalyst except for the total H_2 consumption and the temperature of reduction peaks. On one hand, as listed in Table 5, compared with that of the fresh catalyst, the total H_2 consumption of the Ca poisoned catalysts all are decreased, suggesting the decline of the redox ability of the Ca poisoned catalysts; on the other hand, except that the temperature of the reduction peak T_4 over the four investigated catalysts does not show obvious change, the positions of T_1, T_2, and T_3 over the Ca poisoned catalysts all are shifted to higher values, indicating the active species of the Ca poisoned catalysts are more difficult to be reduced. These results demonstrate that the redox properties of the Ca poisoned catalysts are weakened, which may be another reason for the decreased catalytic activity of the Ca poisoned catalysts.

Results of NH_3-TPD analysis

The NH_3-TPD experiments were carried out to investigate the changes of surface acid sites caused by Ca doping and the results are exhibited in Fig. 8. It can be seen that all the NH_3-TPD curves of the catalysts can be fitted into six sub-peaks in the whole temperature range, which are ascribed to the desorption of the weak adsorbed ammonia (<300 °C) and medium-strong adsorbed ammonia (300–500 °C), respectively.[56,57] Meanwhile, compared with the fresh catalyst, the NH_3-TPD curves of the Ca poisoned catalysts display obvious changes. As listed in Table 6, for one thing, the positions of the corresponding desorption peaks of the Ca poisoned catalysts all are moved to higher values, indicating NH_3 become more difficult to be detached at low temperature; for another, both the weak and the medium surface acid sites of the Ca poisoned are decreased, which suggests that the Ca doping could weaken the adsorption of ammonia over the catalysts. It is well accepted that the adsorption of ammonia is crucial for the SCR reaction and the decreased surface acidity of catalysts will result in the loss of the catalytic activity of catalysts. Thus, the weakened surface acidity of catalysts due to the Ca doping may be responsible for the reduced catalytic activity of catalysts.

Conclusions

The fresh and different Ca poisoned Fe–Ce/Ti catalysts were synthesized and used for the NH_3-SCR reaction. The experimental results show that the Ca doping will lead to a significant decrease in the catalytic activity of catalysts. And based on some physicochemical characterization results, several important conclusions can be drawn as follows:

(1) The Ca doping will lead to smaller specific surface area and pore volume, which will weaken the contact of reactant molecules and active sites and thus decrease the activity of catalysts.

(2) The crystallographic parameter of TiO_2 may not be affected by the Ca doping, while the CeO_2 crystal unit can be expanded due to the Ca^{2+} is partly doped into the original CeO_2 lattice.

(3) The ratios of Fe^{3+}/Fe^{2+} and Ce^{3+}/Ce^{4+} over the Ca poisoned catalysts both are significantly decreased, both of which will result in the drop of the catalytic activity of catalysts.

(4) The addition of Ca could weaken the redox ability and surface acidity of the Ca poisoned catalysts and thus cut down the catalytic performance of catalysts.

Funding information

The authors acknowledge financial support from the National Natural Science Foundation of China (51276039), the Natural Science Foundation of the Jiangsu Higher Education Institutions of China (17KJB610005), the Jiangsu Government Scholarship for Overseas Studies (JS-2018), and the project funded by Nanjing Xiaozhuang University (2019NXY46).

Conflicts of interest

There are no conflicts to declare.

References

1 Q. Liang, J. Li, H. He, T. Yue and L. Tong, *J. Environ. Sci.*, 2020, **90**, 253–261.
2 Y. Jiang, W. Shi, C. Lai, W. Gao, L. Yang, X. Yu, Z. Yang and R. Lin, *J. Energy Inst.*, 2020, **93**, 1332–1340.
3 D. Wang, J. Luo, Q. Yang, J. Yan, K. Zhang, W. Zhang, Y. Peng, J. Li and J. Crittenden, *Environ. Sci. Technol.*, 2019, **53**, 6937–6944.
4 I. Song, H. Lee, S. W. Jeon and D. H. Kim, *J. Catal.*, 2020, **382**, 269–279.
5 L. Liu, K. Xu, S. Su, L. He, M. Qing, H. Chi, T. Liu, S. Hu, Y. Wang and J. Xiang, *Appl. Catal., A*, 2020, **592**, 117413.
6 Y. Zeng, W. Song, Y. Wang, S. Zhang, T. Wang and Q. Zhong, *J. Hazard. Mater.*, 2020, **383**, 121212.
7 R. T. Guo, X. Sun, J. Liu, W. G. Pan, M. Y. Li, S. M. Liu, P. Sun and S. W. Liu, *Appl. Catal., A*, 2018, **558**, 1–8.
8 B. Jia, J. Guo, H. Luo, S. Shu, N. Fang and J. Li, *Appl. Catal., A*, 2018, **553**, 82–90.
9 Y. Jiang, X. Zhang, M. Lu, C. Bao, G. Liang, C. Lai, W. Shi and S. Ma, *J. Taiwan Inst. Chem. Eng.*, 2018, **86**, 133–140.
10 X. Leng, Z. Zhang, Y. Li, T. Zhang, S. Ma, F. Yuan, X. Niu and Y. Zhu, *Fuel Process. Technol.*, 2018, **181**, 33–43.
11 W. Li, C. Zhang, X. Li, P. Tan, A. Zhou, Q. Fang and G. Chen, *Chin. J. Catal.*, 2018, **39**, 1653–1663.
12 Y. Ma, D. Zhang, H. Sun, J. Wu, P. Liang and H. Zhang, *Ind. Eng. Chem. Res.*, 2018, **57**, 3187–3194.
13 C. Pang, Y. Zhuo, Q. Weng and Z. Zhu, *RSC Adv.*, 2018, **8**, 6110–6119.
14 T. Wang, Z. Wan, X. Yang, X. Zhang, X. Niu and B. Sun, *Fuel Process. Technol.*, 2018, **169**, 112–121.
15 Z. Chen, L. Liu, H. Qu, Q. Zhong and Z. Liu, *Catal. Lett.*, 2019, **150**, 514–523.
16 H. I. Hamoud, V. Valtchev and M. Daturi, *Appl. Catal., B*, 2019, **250**, 419–428.
17 Y. Jiang, W. Shi, M. Lu, Q. Li, C. Lai, W. Gao, L. Yang and Z. Yang, *Aerosol Air Qual. Res.*, 2019, **19**, 2381–2386.
18 Q. Li, X. Li, W. Li, L. Zhong, C. Zhang, Q. Fang and G. Chen, *Chem. Eng. J.*, 2019, **369**, 26–34.
19 X. Li, J. Feng, Z. Xu, J. Wang, Y. Wang and W. Zhao, *React. Kinet., Mech. Catal.*, 2019, **128**, 163–174.
20 Z. Song, Y. Xing, T. Zhang, J. Zhao, J. Wang, Y. Mao, B. Zhao, X. Zhang, M. Zhao and Z. Ma, *Appl. Organomet. Chem.*, 2019, **34**, e5446.
21 Y. Wang, L. Xie, F. Liu and W. Ruan, *J. Environ. Sci.*, 2019, **81**, 195–204.
22 X. Li, X. Li, J. Chen, J. Li and J. Hao, *Catal. Commun.*, 2016, **87**, 45–48.
23 L. Chen, J. Li and M. Ge, *Chem. Eng. J.*, 2011, **170**, 531–537.
24 N. Zhu, W. Shan, Y. Shan, J. Du, Z. Lian, Y. Zhang and H. He, *Chem. Eng. J.*, 2020, **388**, 124250.
25 C. U. I. Odenbrand, *Appl. Catal., B*, 2018, **234**, 365–377.
26 H. Chang, C. Shi, M. Li, T. Zhang, C. Wang, L. Jiang and X. Wang, *Chin. J. Catal.*, 2018, **39**, 710–717.
27 S. M. Liu, R. T. Guo, S. X. Wang, W. G. Pan, P. Sun, M. Y. Li and S. W. Liu, *J. Taiwan Inst. Chem. Eng.*, 2017, **78**, 290–298.
28 W. Zhao, Q. Zhong, T. Zhang and Y. Pan, *RSC Adv.*, 2012, **2**, 7906.
29 K. Zhao, J. Meng, J. Lu, Y. He, H. Huang, Z. Tang and X. Zhen, *Appl. Surf. Sci.*, 2018, **445**, 454–461.
30 Y. Li, Y. Li, Y. Wan, S. Zhan, Q. Guan and Y. Tian, *RSC Adv.*, 2016, **6**, 54926–54937.
31 Z. Wang, J. Lan, M. Haneda and Z. Liu, *Catal. Today*, 2020, DOI: 10.1016/j.cattod.2020.05.040.
32 N. Zhu, W. Shan, Z. Lian, Y. Zhang, K. Liu and H. He, *J. Hazard. Mater.*, 2020, **382**, 120970.
33 S. Ma, H. Tan, Y. Li, P. Wang, C. Zhao, X. Niu and Y. Zhu, *Chemosphere*, 2020, **243**, 125309.
34 J. Cheng, L. Song, R. Wu, S. Li, Y. Sun, H. Zhu, W. Qiu and H. He, *J. Rare Earths*, 2020, **38**, 59–69.
35 C. Xu, J. Liu, Z. Zhao, F. Yu, K. Cheng, Y. Wei, A. Duan and G. Jiang, *J. Environ. Sci.*, 2015, **31**, 74–80.
36 M. Zabilskiy, B. Erjavec, P. Djinović and A. Pintar, *Chem. Eng. J.*, 2014, **254**, 153–162.
37 A. Kambolis, H. Matralis, A. Trovarelli and C. Papadopoulou, *Appl. Catal., A*, 2010, **377**, 16–26.
38 V. J. Ferreira, P. Tavares, J. L. Figueiredo and J. L. Faria, *Ind. Eng. Chem. Res.*, 2012, **51**, 10535–10541.
39 M. Schwidder, M. Kumar, K. Klementiev, M. Pohl, A. Bruckner and W. Grunert, *J. Catal.*, 2005, **231**, 314–330.
40 M. Iwasaki, K. Yamazaki, K. Banno and H. Shinjoh, *J. Catal.*, 2008, **260**, 205–216.
41 H. Jouini, I. Mejri, C. Petitto, J. Martinez-Ortigosa, A. Vidal-Moya, M. Mhamdi, T. Blasco and G. Delahay, *Microporous Mesoporous Mater.*, 2018, **260**, 217–226.
42 L. Zhong, Q. Fang, X. Li, Q. Li, C. Zhang and G. Chen, *Appl. Catal., A*, 2019, **579**, 151–158.
43 N. Fang, J. Guo, S. Shu, H. Luo, Y. Chu and J. Li, *Chem. Eng. J.*, 2017, **325**, 114–123.
44 G. Delahay, D. Valade, A. Guzmanvargas and B. Coq, *Appl. Catal., B*, 2005, **55**, 149–155.
45 F. Xia, Z. Song, X. Liu, X. Liu, Y. Yang, Q. Zhang and J. Peng, *Res. Chem. Intermed.*, 2018, **44**, 2703–2717.

46 N. S. Ferreira, R. S. Angélica, V. B. Marques, C. C. O. de Lima and M. S. Silva, *Mater. Lett.*, 2016, **165**, 139–142.
47 C. Liu, G. Gao, J.-W. Shi, C. He, G. Li, N. Bai and C. Niu, *Catal. Commun.*, 2016, **86**, 36–40.
48 P. Ning, Z. Song, H. Li, Q. Zhang, X. Liu, J. Zhang, X. Tang and Z. Huang, *Appl. Surf. Sci.*, 2015, **332**, 130–137.
49 C. Liu, L. Chen, H. Chang, L. Ma, Y. Peng, H. Arandiyan and J. Li, *Catal. Commun.*, 2013, **40**, 145–148.
50 L. Jiang, Q. Liu, G. Ran, M. Kong, S. Ren, J. Yang and J. Li, *Chem. Eng. J.*, 2019, **370**, 810–821.
51 X. Xu, J. Enchen, W. Mingfeng, L. Bosong and Z. Ling, *Renewable Energy*, 2012, **41**, 23–28.
52 H. J. Wan, B. S. Wu, C. H. Zhang, H. W. Xiang, Y. W. Li, B. F. Xu and F. Yi, *Catal. Commun.*, 2007, **8**, 1538–1545.
53 A. P. Wimmers, J. A. Moulijn, *et al.*, *J. Phys. Chem.*, 1986, **90**, 1331–1337.
54 H. Chen, Y. Xia, H. Huang, Y. Gan, X. Tao, C. Liang, J. Luo, R. Fang, J. Zhang, W. Zhang and X. Liu, *Chem. Eng. J.*, 2017, **330**, 1195–1202.
55 S. Yang, Y. Guo, H. Chang, L. Ma, Y. Peng, Z. Qu, N. Yan, C. Wang and J. Li, *Appl. Catal., B*, 2013, **136–137**, 19–28.
56 J. Miao, H. Li, Q. Su, Y. Yu, Y. Chen, J. Chen and J. Wang, *Catal. Commun.*, 2019, **125**, 118–122.
57 H. Xu, Y. Li, B. Xu, Y. Cao, X. Feng, M. Sun, M. Gong and Y. Chen, *J. Ind. Eng. Chem.*, 2016, **36**, 334–345.